Biomaterials Science

ROYAL SOCIETY OF CHEMISTRY

PAPER

View Article Online
View Journal | View Issue

Cite this: *Biomater. Sci.*, 2025, **13**, 6791

Polyaspartic acid coatings for blood-contacting surfaces: Promising antithrombotic and antibacterial properties under static and dynamic conditions

Cuong Hung Luu, [a,b] Dimple Sajin,[a,b] Hoang Huy Vu,[b,c] Nhat-Khuong Nguyen,[b] Nam-Trung Nguyen [b] and Hang Thu Ta *[a,b]

The increasing use of blood-contacting medical devices has brought about significant advancements in patient care, yet it also presents challenges such as thrombus formation and infection risks. Surface coatings play a vital role in mitigating these side effects, enhancing the safety and effectiveness of such devices. In this study, we introduced a novel coating employing poly(aspartic acid) (PASP), which can be easily applied through various modification pathways. PASP has demonstrated the ability to resist surface coagulation and exhibited antibacterial properties *in vitro* under both static and dynamic flow conditions. The results showed that PASP coatings significantly reduced platelet adhesion and thrombus formation, with the blood clot area percentage being reduced to 1.0 ± 0.5% from 9.7 ± 4.6% on uncoated surfaces. Furthermore, PASP coatings showed a notable reduction in *E. coli* adhesion, with bacterial levels decreasing to 71.5 ± 12.6%. These findings suggest that PASP is a promising candidate for enhancing the biocompatibility and functionality of blood-contacting medical devices, with potential for further development in antibacterial and antithrombotic applications.

Received 25th December 2024,
Accepted 10th August 2025

DOI: 10.1039/d4bm01714e

rsc.li/biomaterials-science

1. Introduction

The advancement of medical technology has led to the increasing use of devices that interact directly with blood, such as catheters, stents, haemodialysis membranes, and heart valves.[1,2] While these devices have significantly improved patient outcomes and enabled more advanced treatments, their interaction with blood presents a critical challenge—surface-induced thrombus formation.[2,3] Indeed, when blood comes in contact with artificial surfaces, it triggers a cascade of biological responses that can lead to the formation of blood clots on the device's surface, a phenomenon known as thrombosis.[1–3] This thrombus formation, even in a smaller scale compared to arterial thrombosis, can cause serious complications, including device malfunction, increased risk of infection, and blockage of blood flow, which can potentially lead to life-threatening conditions such as stroke, heart attack, or pulmonary embolism.[4–7] Moreover, the formation of blood clots necessitates the use of anticoagulant drugs, which can lead to systemic side effects such as bleeding and can compromise the overall safety of the medical intervention.[8,9] As a result, addressing surface-induced thrombosis remains a critical goal in the development and improvement of blood-contacting medical devices.

Several factors contribute to surface-induced thrombus formation, rooted in the complex biological reactions that occur when blood encounters foreign materials.[10–12] The body's natural response to foreign surfaces involves the activation of platelets, coagulation cascades, and inflammatory pathways, which together promote clot formation as a protective mechanism.[10,13,14] The material properties of the device surface, including its roughness, hydrophobicity, and chemical composition, play significant roles in determining the extent of thrombus formation. Rough or hydrophobic surfaces are particularly more likely to initiate protein adsorption, platelet adhesion, and subsequent clot formation.[1,15] Various strategies have been developed to mitigate these adverse reactions. One of the most effective approaches is surface modification.[1,9] By altering the surface properties of medical devices, researchers aim to create a more biocompatible interface that reduces the risk of thrombus formation.[13,16] In particular, surface coatings have gained prominence due to their

[a]*School of Environment and Science, Griffith University, Nathan, QLD 4111, Australia. E-mail: h.ta@griffith.edu.au; Tel: +61 (7) 3735 5384, https://hangta.group/; https://experts.griffith.edu.au/27034-hang-ta*
[b]*Queensland Quantum and Advanced Technologies Research Institute, Griffith University, Nathan, QLD 4111, Australia*
[c]*School of Engineering and Built Environment, Griffith University, Nathan, QLD 4111, Australia*

ability to provide a physical and chemical barrier between blood and the underlying material. These coatings can be designed to prevent protein adsorption, inhibit platelet adhesion, and regulate the immune response, thereby significantly reducing the risk of thrombosis without the need for systemic anticoagulants.[17,18]

Polymers have emerged as a versatile and effective class of surface coating materials due to their tunable properties and ability to be engineered for specific biological interactions, offering unique advantages in modifying surface interactions with blood.[19–21] Hydrophilic polymers particularly have been widely explored for their ability to create a hydrated layer on the device surface that prevents protein and platelet adhesion. This characteristic makes hydrophilic polymer coatings a preferred direction in the development of antithrombotic surfaces.[2,19,20] One of such hydrophilic polymers that has garnered attention in recent years is poly(aspartic acid) (PASP). PASP is an anionic polyelectrolyte that is biodegradable, biocompatible, and relatively easy to synthesise.[22] PASP is derived from aspartic acid, a naturally occurring amino acid, making it an environmentally friendly option for medical applications.[23] Its polyanionic nature enables its interaction with biological molecules and cells in a manner that can prevent clot formation and reduce the risk of thrombosis. Additionally, PASP has shown promise as an antibacterial agent due to its charge interactions with bacterial cell membranes, which could further enhance its utility as a surface coating material in medical devices prone to infection.[24] Given its favorable properties, PASP presents its significant potential as a novel coating material for reducing thrombus formation on blood-contacting medical devices.

In this study, we proposed the use of PASP as a surface coating material for blood-contacting medical devices to reduce thrombus formation and enhance biocompatibility. The study focuses on the mussel-inspired coating methods and characterisation of PASP coatings, and evaluates their antithrombosis capabilities *in vitro* using established blood compatibility assays. We also assessed the antithrombotic efficacy of PASP coatings under dynamic flow conditions to ensure their suitability for use in a real scenario by using a microfluidic device model. Furthermore, the potential antibacterial properties of PASP coatings were investigated, providing a comprehensive evaluation of PASP as a multifunctional surface modification strategy. Through this research, we aim to establish PASP as a promising candidate for improving the performance and safety of medical devices, particularly in applications where blood compatibility and infection resistance are of paramount importance.

2. Materials and methods

2.1. Materials

L-Aspartic acid (≥98%), phosphoric acid (H_3PO_4, ≥85%), sulfolane ($C_4H_8O_2S$, ≥99%), and sodium hydroxide (NaOH, ≥98%) were obtained from Merck (Darmstadt, Germany). Dimethyl sulfoxide (DMSO, ≥99.9%), *N*,*N*-dimethylformamide (DMF, ≥99%), phosphate-buffered saline (PBS, pH 7.4, 10× solution), Triton X-100 (≥99%) and dopamine hydrochloride (DA, ≥98%) were purchased from Sigma-Aldrich (MO, USA). Tris(hydroxymethyl)aminomethane (Tris, ≥99%), methanol (≥99.9%), and ethanol (≥99.8%) were provided by Thermo Fisher Scientific (MA, USA). The chemicals and solvents were used immediately upon purchase without undergoing any additional purification procedures. Whole blood was obtained from healthy volunteers under human ethics approval by the Griffith University Human Ethics Committee (approval number: 2021/598).

2.2. Characterisation methodologies

UV-Vis spectroscopy. A UV-Vis spectrophotometer (CLARIOstar Plus Microplate Reader, BMG Labtech, Germany) was employed to determine the absorption spectra of compounds, particularly dopamine conjugates, and to quantify the dopamine content attached to the PSI chain. Furthermore, UV-Vis spectroscopy was used to measure the haemoglobin content following erythrocyte lysis.

Fluorescence spectroscopy. A CLARIOstar was used to measure the fluorescence intensity of the assays conducted in this study.

Optical microscopy. Fluorescence microscopy (CKX53 cell culture microscope with a DP74 microscope digital camera, Olympus Corporation, Japan) was employed to observe adhered platelets under dynamic conditions using a microfluidic device. Additionally, thrombus formation was observed using bright-field microscopy.

FTIR spectroscopy. Attenuated total reflectance Fourier-transform infrared spectroscopy (ATR-FTIR, Spectrum Two FT-IR, PerkinElmer, United States) was employed to analyse the chemical bonds of PSI, PASP, and the fabricated surface coatings. For the FTIR spectra of the surface coatings, the substrate material was measured as the background, and the final results were subtracted from the background to minimise noise signals.

^{1}H NMR spectroscopy. Proton nuclear magnetic resonance spectroscopy (^{1}H NMR, Bruker Avance III HD console, Bruker Corporation, Germany) was used to elucidate the structural formula of polymeric compounds, such as PSI and PASP, post-synthesis. DMSO-d_6 was employed as the solvent to disperse the polymers, given its ability to dissolve both PSI and PASP.

Contact angle measurement. To assess the success of the coating, water contact angle (WCA) measurements were conducted to demonstrate the changes in surface tension before and after polymeric surface coating. Specifically, 10 μL of Milli-Q water was automatically dispensed onto bare or coated surfaces. After a 10-second settling period, a tensiometer (Theta Flow, Biolin Scientific, Sweden) was used to measure the WCA and capture an image of the water droplet for reference.

Morphology. The surface morphology of the coating was analysed using a scanning electron microscope (SEM, JSM-6510, JEOL Ltd, Japan). To enhance visibility, the coated samples were sputter-coated with pure gold for 1 minute before imaging.

2.3. Synthesis of PSI and PASP

To synthesise polysuccinimide (PSI), L-aspartic acid was polymerised in sulfolane solvent, catalysed by phosphoric acid.[25,26] In summary, aspartic acid (14 g, M_W = 133.1 g mol^{-1}, 105.18 mmol), phosphoric acid (85% by weight in H_2O, 1 mL), and sulfolane (56 mL) were added to a 100 mL flask, which was then placed in an oil bath and heated to 180 °C under a nitrogen gas flow, with mechanical stirring at 150 rpm. The mixture was stirred for 5 hours before the flask was removed from the oil bath and allowed to cool to room temperature. The resulting solution was then precipitated in a large volume of deionised water (DIW) and left to stand for 2 hours. The precipitated polymer (PSI) was collected by centrifugation at 5000 × *g* for 10 minutes, redispersed with DIW, and repeated four times to remove any unreacted starting materials and residual solvent. The PSI precipitate was subsequently collected by centrifugation at 5000 × *g* once more, and then dried in a vacuum oven at 60 °C for 4 days. The dried PSI powder was stored in a desiccator until required for further use.

PSI was hydrolysed to poly(aspartic acid) using NaOH. Specifically, NaOH (50 mg, M_W = 39.997 g mol^{-1}, 1.25 mmol) was added to PSI powder (100 mg, M_W of succinimide = 97.09 g mol^{-1}, 1.03 mmol) in 5 mL of water and stirred at room temperature for 2 hours. The resulting product, sodium polyaspartate, was precipitated in methanol and washed several times by centrifugation at 5000 × *g* for 10 minutes to remove any excess NaOH. Finally, the product was freeze-dried to obtain the final material, namely PASP.

2.4. Modification of PSI with dopamine

Dopamine was conjugated to PSI *via* a ring-opening reaction to introduce the adhesion property of dopamine to PSI and thereby improve the coating's effectiveness.[27] This process involved the amine group of dopamine attacking the succinimide ring of PSI. Specifically, PSI (containing 10 mmol of succinimide groups) was dissolved in 5 mL of DMSO in a three-necked round-bottom flask, which was degassed with nitrogen for 30 minutes. Pyridine (200 μL) and dopamine were then added to the solution, and the ratio of PSI to dopamine is presented in Table 1. The reaction was conducted at room temperature, in the dark, for 5 hours with continuous stirring. Upon completion of the reaction, the mixture was precipitated in DIW and the resulting precipitate was collected by centrifugation at 5000 × *g* for 10 minutes. The precipitate was then washed several times with DIW to eliminate any unreacted starting materials. Following the washing process, the precipitate was dried in a vacuum oven at 40 °C until a constant weight was achieved. The modified PSI, referred to as PSI-DA, was stored in a desiccator until required for further use.

Table 1 Grafting ratio of dopamine moieties on the PSI chain

	Succinimide (mmol)	DA (mmol)	DA content (%)
PSI	10	0.0	0
PSI-DA$_5$	10	0.5	5
PSI-DA$_{10}$	10	1.0	10
PSI-DA$_{20}$	10	2.0	20

2.5. PASP coating *via* the direct method

In the direct coating method, PSI-DA with varying degrees of conjugation was employed for the study. Initially, the surfaces were cut into small pieces using a hole puncher and cleaned according to the procedure outlined in section 2.7 before the coating process. PSI-DA (150 mg) was then dissolved in 2 mL of DMF, after which the solution was diluted to a concentration of 10 mg mL^{-1} using Tris-HCl buffer at pH 8.5. The substrates were immediately immersed in this solution for 2 hours to achieve coating. Following the coating process, the surfaces were pre-rinsed with DIW to remove any unreacted impurities. Finally, the surfaces were immersed in a 1 M NaOH solution to hydrolyse the succinimide groups of PSI-DA, resulting in the formation of PASP-DA coated surfaces, denoted as (PASP-DA). We conducted experiments on four different substrate materials: PET, PVC, PDMS, and glass to affirm the universal adhesion properties of dopamine moieties on PSI-DA.

2.6. PASP coating *via* the indirect method

In the indirect coating method, the substrate surfaces were initially coated with a layer of polydopamine *via* the classical polydopamine deposition reaction.[28] Briefly, dopamine was dissolved in Tris-HCl buffer solution at pH 8.5 to a concentration of 2 mg mL^{-1}, denoted as (PDA). The surfaces were then immersed in this solution for 2 hours. After rinsing with deionised water, the surfaces were subsequently soaked in a PSI solution in DMF at a concentration of 10 mg mL^{-1}, namely (PSI). The reaction was carried out at room temperature under dark conditions to obtain the PSI-coated surfaces. Following the removal of PSI coating solution, these surfaces were then hydrolysed in an alkaline environment using 1 M NaOH for 30 minutes, resulting in PASP-coated surfaces, so-called (PASP).

This method was also applied to coat the surfaces of microfluidic devices. Similarly, the 5 mL PSI solution (10 mg mL^{-1}) was circulated in the coating process for 2 hours *via* a close dynamic flow governed by a peristaltic pump at a moderate flow rate of 100 μL min^{-1} to prevent material abrasion, ensuring the integrity of the coating. Then the washing process was conducted using DIW for 10 minutes with a peristaltic pump.

2.7. Sterilisation of surface coatings

Before coating the surfaces with the material, they were first cleaned with 70% alcohol and then air-dried, followed by storage in a sealed container until use. A similar procedure was applied when preparing samples for *in vitro* studies. Prior to conducting *in vitro* experiments, the samples were equilibrated in PBS for 30 minutes. For the WCA measurement samples, the substrates were rinsed with DIW to ensure accuracy.

2.8. Protein binding capacity of PASP coatings

Albumin and fibrinogen play crucial roles in surface-induced blood coagulation, where fibrinogen, when adsorbed onto surfaces, can readily trigger the activation of other clotting

factors, leading to blood clot formation. Conversely, albumin is believed to have an opposing effect, as it can inhibit the adsorption of fibrinogen on surfaces. Therefore, this assessment method is pivotal for evaluating the potential for surface-induced blood clot formation. In this study, albumin and fibrinogen were first dissolved in PBS buffer at pH 7.4, at concentrations of 50 and 5 mg mL^{-1}, respectively, to mimic the relative protein concentrations found in human blood.[29,30] Subsequently, coated and uncoated substrates were placed into a 96-well plate, followed by the addition of the protein solutions mentioned above, and incubated at 37 °C for 2 hours. After incubation, the surfaces were rinsed with PBS to remove any non-adherent proteins. The amount of protein adsorbed onto the surfaces was then quantified using the MicroBCA assay at a wavelength of 562 nm.

2.9. Platelet adhesion on PASP coatings

Platelet adhesion was assessed using platelet-rich plasma (PRP) applied to the surface to evaluate the platelet adherence capacity. Initially, PRP was isolated from whole blood through centrifugation at 1500 rpm. The upper plasma layer was carefully separated and transferred to a new container, designated as PRP. PRP was then refilled with PBS buffer at pH 7.4 to restore the platelet concentration to levels similar to those found in whole blood. 100 μL of the diluted solution was pipetted onto the surfaces in a 96-well plate, which were then incubated at 37 °C for 2 hours. After incubation, the samples were washed once with PBS to remove any non-adherent platelets, followed by staining mitochondria in platelets with 100 μL of 3,3′-dihexyloxacarbocyanine iodide (DiOC6) in PBS at a concentration of 1 μg mL^{-1}. Finally, the fluorescence intensity was measured at an emission wavelength of 510 nm and an excitation wavelength of 470 nm to quantify the amount of platelet adhesion on the surface.

2.10. Activated partial thromboplastin time of PASP coatings

Activated partial thromboplastin time (APTT) was assessed using platelet-poor plasma (PPP), which was obtained by centrifuging whole blood at 3000 rpm for 15 minutes.[31] The surface was first equilibrated in PBS at pH 7.4 for 30 minutes. After equilibration, PBS was discarded and 45 μL of PPP was mixed with an equal volume of the APTT reagent (Dade® Actin® FSL). This mixture was then applied to the surface and incubated at 37 °C for 15 minutes. Following incubation, 90 μL of the mixture was transferred to new wells in a well plate, which was subsequently placed in a plate reader. To initiate the clotting process, 10 μL of $CaCl_2$ solution at a concentration of 0.25 mol L^{-1} was added to the mixture. The APTT was then measured by the turbidimetric method using the microplate reader at a wavelength of 600 nm.[32] Herein, the clotting time was determined as the lag time before a sharp increase in absorbance occurred.[33]

2.11. Biocompatibility of PASP coatings

The biosafety of the surface was evaluated *in vitro* using endothelial cells, as these are the primary cell type in direct contact with blood-interacting materials. For this study, endothelial cells (SVEC4-10, ATCC CRL-2181) were employed. These cells were cultured in low glucose Dulbecco's modified Eagle's medium (DMEM), which was supplemented with 10% fetal bovine serum (FBS) and 1% penicillin–streptomycin (P/S, 10 000 U mL^{-1}) and maintained at 37 °C in humidified air containing 5% CO_2.[34] Initially, 100 μL of SVECs, at a concentration of 10^4 cells per mL, were seeded into each well and incubated at 37 °C under 5% CO_2 for 24 hours. Subsequently, sterilised substrates were introduced into the wells containing the cells and incubated for an additional 24 hours. To assess cell viability, the PrestoBlue™ assay was employed following the manufacturer's standard protocol. After adding PrestoBlue™ solution to new wells, the absorbance of each well was measured at 570 nm using a microplate reader. The data were then statistically analysed to evaluate the impact of the coating layers on SVEC viability.

2.12. Antibacterial efficacy of PASP coatings

The anti-adhesion properties against *Escherichia coli* (*E. coli*, ATCC 25922) and *Staphylococcus aureus* (*S. aureus*, ATCC 23235) were evaluated on both coated and uncoated surfaces, with antibiotics serving as a positive control. Initially, bacteria were cultured in nutrient broth for 8 hours, achieving a bacterial density of 5×10^6 CFU mL^{-1}. The surfaces were then equilibrated in PBS for 30 minutes before being placed into 96-well plates, followed by the addition of 100 μL of the bacterial suspension. PET served as the control surface, while kanamycin at a concentration of 0.25 mg mL^{-1} was used as the positive control for comparison. After incubation at 37 °C for 2 hours, the surfaces were rinsed with PBS to eliminate non-adherent bacteria. The quantity of bacteria remaining attached to the surface was subsequently quantified using the PrestoBlue™ assay as previously described.

2.13. Haemolytic activity of PASP coatings

Haemocompatibility testing of the surface coatings was carried out using human blood to evaluate its haemolytic potential. Whole blood was obtained from healthy volunteers with informed consent (Australian Red Cross) under the guidelines of human ethics approval by the Griffith University Human Ethics Committee (approval number: 2021/598). Initially, 3.5 mL of blood collected in a 3.2% citrate tube was centrifuged at 3000 rpm for 15 minutes to separate the plasma, which was subsequently removed. The underlying red blood cell (RBC) layer was carefully collected and washed twice with PBS at pH 7.4. The RBCs were then diluted with PBS to create a 4% solution. A volume of 500 μL of this suspension was transferred into Eppendorf tubes containing either substrates, positive, or negative controls. For the positive control, 1% Triton X-100 was used, while PBS at pH 7.4 served as the negative control. The tubes were incubated at 37 °C for 4 and 24 hours. Following incubation, the samples were centrifuged, and the supernatant was collected for analysis *via* UV-Vis spectroscopy at 540 nm. The degree of

haemolysis was calculated using a standard formula given below.[14,35–39]

$$\text{Haemolysis ratio}\,(\%) = \frac{\text{OD}_{\text{sample}} - \text{OD}_{\text{negative}}}{\text{OD}_{\text{positive}} - \text{OD}_{\text{negative}}} \times 100\% \quad (1)$$

2.14. Fabrication of the single channel microfluidic device

In this study, PDMS microfluidic devices were used as a robust *in vitro* model to mimic the dynamic conditions of blood vessels. The mould for the single-channel device, previously developed by our group, featured dimensions of 255 μm in width, 110 μm in height, and 20 mm in length. A mixture of PDMS and curing agent from the SYLGARD™ 184 Silicone Elastomer Kit was thoroughly combined and poured into the mould. Desiccation was performed prior to placing the mould in an oven at 60 °C to expedite the polymer curing process. Once cured, the PDMS chips were bonded to glass slides using oxygen plasma treatment for 1.5 minutes. The subsequent coating procedures were conducted as outlined in section 2.6.

2.15. Platelet adhesion under dynamic flow

Microfluidic devices, both coated and uncoated, were utilised to assess platelet adhesion under physiological flow conditions. The flow rate was set at 31 μL min^{-1} based on physiological shear (1000 s^{-1}) with the detailed calculations provided in the Supplementary Information (SI), and the experiment was conducted over a period of 2 hours, with the flow rate calculations provided in the SI. Initially, whole blood was centrifuged to isolate PRP. The volume ratio of blood plasma to RBCs was nearly 1 : 1. Therefore, PRP was then diluted 1 : 1 with PBS to match the platelet concentration found in whole blood in the first place. Following dilution, PRP was incubated with DiOC6 at a concentration of 0.1 mg mL^{-1}, using a volume ratio of 1 : 200, for 20 minutes in a 37 °C incubator with gentle shaking at 50 rpm. The DiOC6-stained platelets were subsequently perfused through the microfluidic device using a syringe pump. In this setup, the inlet of the microfluidic chip was connected to the pump, while the outlet was headed to waste disposal. This procedure was repeated three times across three separate channels, with observations made using a fluorescence microscope. Fluorescence intensity per area with a standardised size of 532 544.4 μm^2 was determined from five distinct images captured under the microscope, using ImageJ software. A comparison graph was generated to analyse the differences between coated and uncoated devices.

2.16. Thrombus formation under dynamic flow

In a similar manner to the experiment of platelet adhesion under flow conditions, the formation of whole blood clots was assessed using a single-channel microfluidic device with a width of 255 μm, a height of 110 μm, and a length of 20 mm. Whole blood was collected directly from donors and subsequently diluted twice with PBS at pH 7.4 before being transferred to a syringe for flow experiments. This approach ensured both thrombus formation within the channel and facilitated the observation of clot development on the surface. The diluted blood was then perfused through the microfluidic device at a flow rate of 31 μL min^{-1} using a syringe pump. After each 2-hour flow experiment, the entire channel was inspected for blood clot formation. To ensure reproducibility, the experiment was repeated three times across different channels. Microscopic methods of the blood clots were subsequently processed using ImageJ software developed by Kenry *et al.* to quantify the blood clot area percentage within the standardised area of 532 544.4 μm^2 throughout five distinct images.[40]

2.17. Statistical analysis

In our study, all experimental procedures were replicated at least three times ($n = 3$) to ensure the robustness and reliability of the results. The data presented are the mean values ± standard deviations. Graph plotting and statistical analyses were conducted using GraphPad Prism software, version 10.2, using unpaired *t*-tests and one-way ANOVA to determine the statistical significance across various datasets. Significance levels were classified as follows: not significant (ns) for *p*-values ≥ 0.05, * for $p < 0.05$, ** for $p < 0.01$, *** for $p < 0.001$, and **** for $p < 0.0001$.

3. Results and discussion

3.1. Characterisation of PSI and PASP polymers

In this study, we primarily used two types of polymers: polysuccinimide (PSI) and poly(aspartic acid) (PASP). PASP, the main focus of this research, was evaluated for its potential applicability in surface coating with anticoagulant properties. Conversely, PSI, synthesised using the method outlined in the article, served as a crucial intermediate for the production of PASP. As such, both polymers underwent chemical analysis to confirm the successful completion of the synthesis reaction.

The synthesis process of PASP is illustrated in Fig. 1A, where PSI is first synthesised from the monomer L-aspartic acid, a non-essential amino acid naturally produced by mammals, ensuring its safety for biological applications. PSI synthesis occured *via* a condensation dehydration reaction, resulting in a polymer containing two types of succinimide units, differentiated by their linkage positions. PASP was subsequently derived through the alkaline hydrolysis of PSI, which produced a polymer chain featuring both α- and β-linkages of the aspartic acid units. Fig. 1B presents the chemical bonds of PSI and PASP, clearly characterised in their FTIR spectra. Both polymers exhibited signals in the region above 3000 cm^{-1}, characterised by a broad trough that reflected overlapping absorptions of N–H and/or O–H bonds. Additionally, both spectra showed absorption features corresponding to C–H bonds around 2954 cm^{-1}. For PSI, a distinct absorption at 1734 cm^{-1} was observed, indicating the presence of imide bonds, a characteristic feature of PSI, consistent with previously reported studies.[27] In contrast, the spectrum of PASP after hydrolysis revealed overlapping amide bands I and

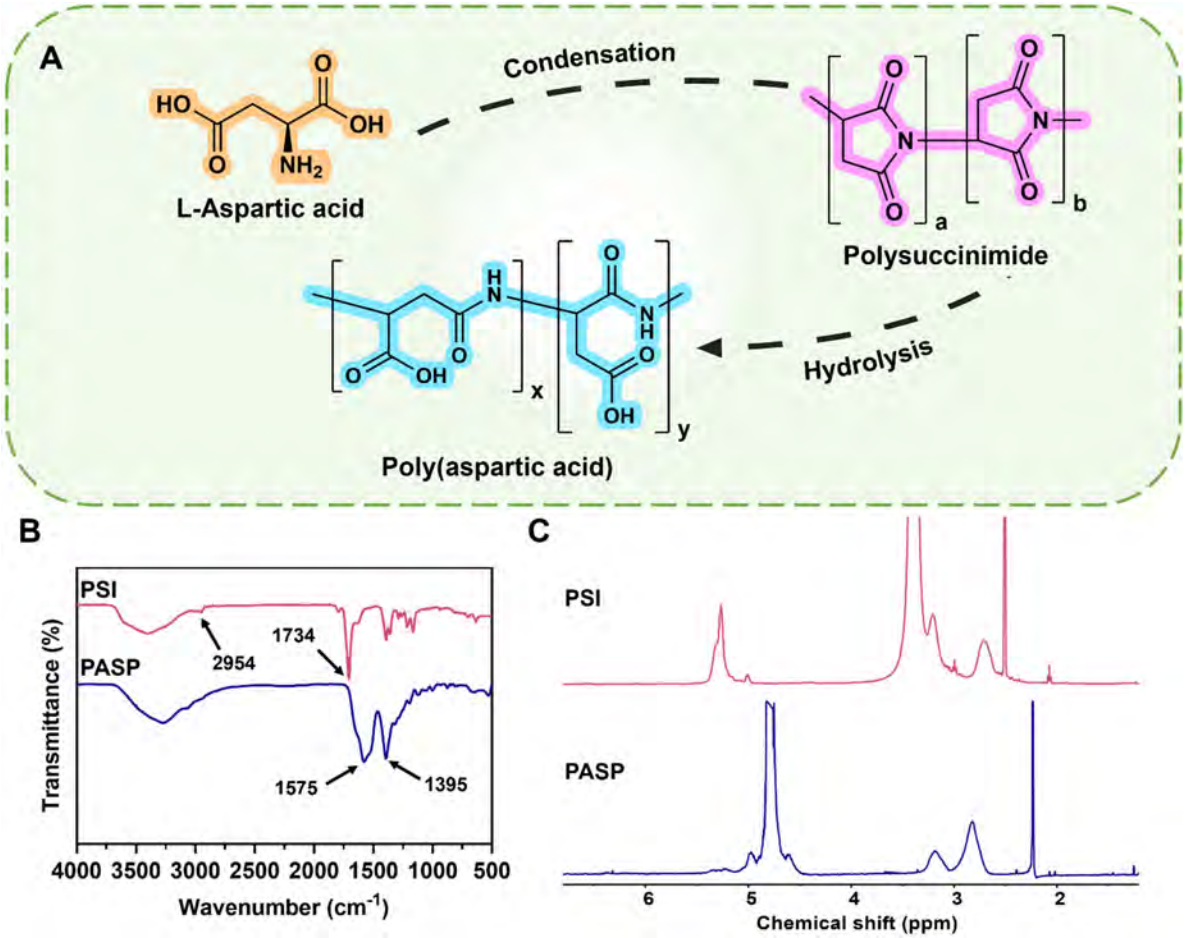

Fig. 1 Synthesis of PSI and PASP polymers *via* the polycondensation method. (A) Schematic procedure of the synthesis process of PASP from L-aspartic acid *via* intermediate PSI; (B) FTIR and (C) ^{1}H NMR spectra of PSI and PASP.

II around 1600 cm^{-1}. Notably, the amide II band at 1575 cm^{-1}, indicative of C–N stretching and N–H bending vibrations, appeared with high intensity, which was absent in the PSI spectrum. Furthermore, the enhanced O–H bending vibration at 1395 cm^{-1} signified hydrolysis and the formation of carboxyl groups in PASP.

Additionally, ^{1}H NMR spectra were acquired to further verify the chemical structures of PSI and PASP. The ^{1}H NMR spectrum of PSI displayed characteristic peaks at 2.7 ppm, 3.2 ppm, and 5.2 ppm, corresponding to the protons in the methylene and methine groups of the succinimide units. Strong signals at 2.5 ppm and 3.3 ppm were attributed to residual DMSO-d_6 solvent and water absorbed by the PSI polymer powder. In comparison, the NMR spectrum of PASP exhibited the expected chemical shifts at 2.2 ppm, 2.8 ppm, and 3.2 ppm, attributed to the protons in methylene and methine groups, further confirming the structural composition of the polymers.[41,42] Collectively, the characterisation results affirmed that PSI and PASP possess well-defined structures, demonstrating the successful synthesis of both polymers, consistent with findings from previous studies.[27,43] In summary, the spectral analysis outcomes presented above confirm the successful synthesis of the polymer, indicating its potential for application with additional modifications.

3.2. Modification of polysuccinimide with dopamine

In the literature, dopamine (DA) is frequently employed in surface coatings owing to its bio-inspired adhesive properties that emulate the potent adhesive proteins found in mussels.[44,45] This biomimetic approach enables DA to establish robust coatings that adhere effectively to diverse surface materials, thereby enhancing their functionality and biocompatibility, as depicted in Fig. 2C. In our study, we leveraged the outstanding adhesive properties of DA, particularly modifying the PSI backbone to synthesise precursors for surface coating applications. Notably, this method facilitates straightforward conjugation through a ring-opening reaction of succinimide, which readily bonds with the amino group of DA without requiring catalysts, unlike traditional carboxyl-amino reactions.

We employed various analytical techniques to assess the properties and to confirm the molecular structure of the PSI-DA precursors. Initially, the absorption spectra of these precursors were recorded using UV-Vis spectroscopy (Fig. 2A).

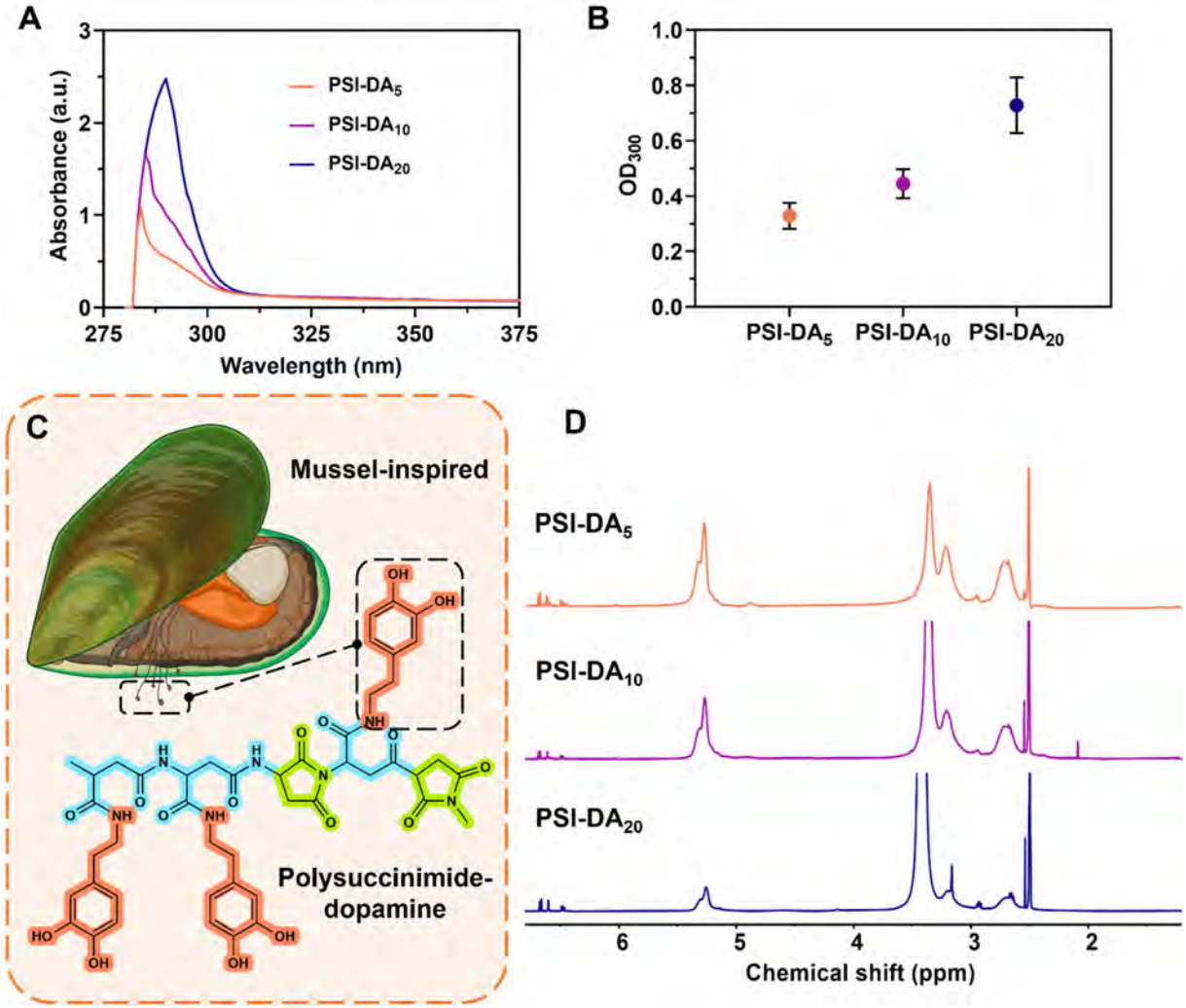

Fig. 2 Dopamine conjugation of PSI. (A) UV-Vis spectra of PSI-DAs at the same concentration of 2 mg mL^{-1}; (B) optical density of PSI-DAs at 300 nm (2 mg mL^{-1}); (C) depiction of the mussel-inspired properties of DAs illustrating universal adhesion benefits for surface coatings; (D) ^1H NMR spectra of precursor PSI-DAs, dissolved in DMSO-d_6 solvent.

The spectra for all three precursors displayed a predominant absorption peak at approximately 280 nm and another overlapping peak at around 300 nm, attributed to the absorption of PSI and conjugated π bonds in DA moieties, respectively. This was corroborated by the spectra of pristine PSI and DA presented in Fig. S1. Further analysis measured the optical density (OD) of PSI-DA at 300 nm, with results from different synthesis batches, indicating that the absorption intensity increased proportionally with the DA content used, as detailed in Table 1. Additionally, the conjugates were analysed using a ^1H NMR spectrometer. While the characteristic peaks of the PSI backbone remained consistent, signals attributable to dopamine moieties were observed above 6.5 ppm, corresponding to protons in catechol groups. The intensity of these peaks clearly increased with the amount of dopamine incorporated. Nevertheless, the degree of dopamine grafting on the PSI polymer proved challenging to be quantified precisely using standard proton spectral curves due to peak overlap. The aforementioned results also substantiate the presence of DA groups on PSI, which is expected to enhance adhesion during surface coating processes.

3.3. Universal adhesion of DA and coating strategies

As noted previously, the reactive nature of intermediates such as PSI allows for easy modification of functionalities, motivating us to propose two potential coating strategies for the material. Initially, the pre-synthesised PSI-DAs were employed in the "direct method", wherein the PSI-DA precursors were directly applied to the surface coating, with the schematic reaction depicted in Fig. S2. This approach also facilitates the assessment of adhesion capabilities across different material surfaces. Glass, being the most polar surface, moderately polar PET and PVC, and hydrophobic PDMS were selected due to their diverse surface properties and their relevance in both research and practical applications. As illustrated in Fig. 3A, the water contact angle (WCA), indicative of the surface

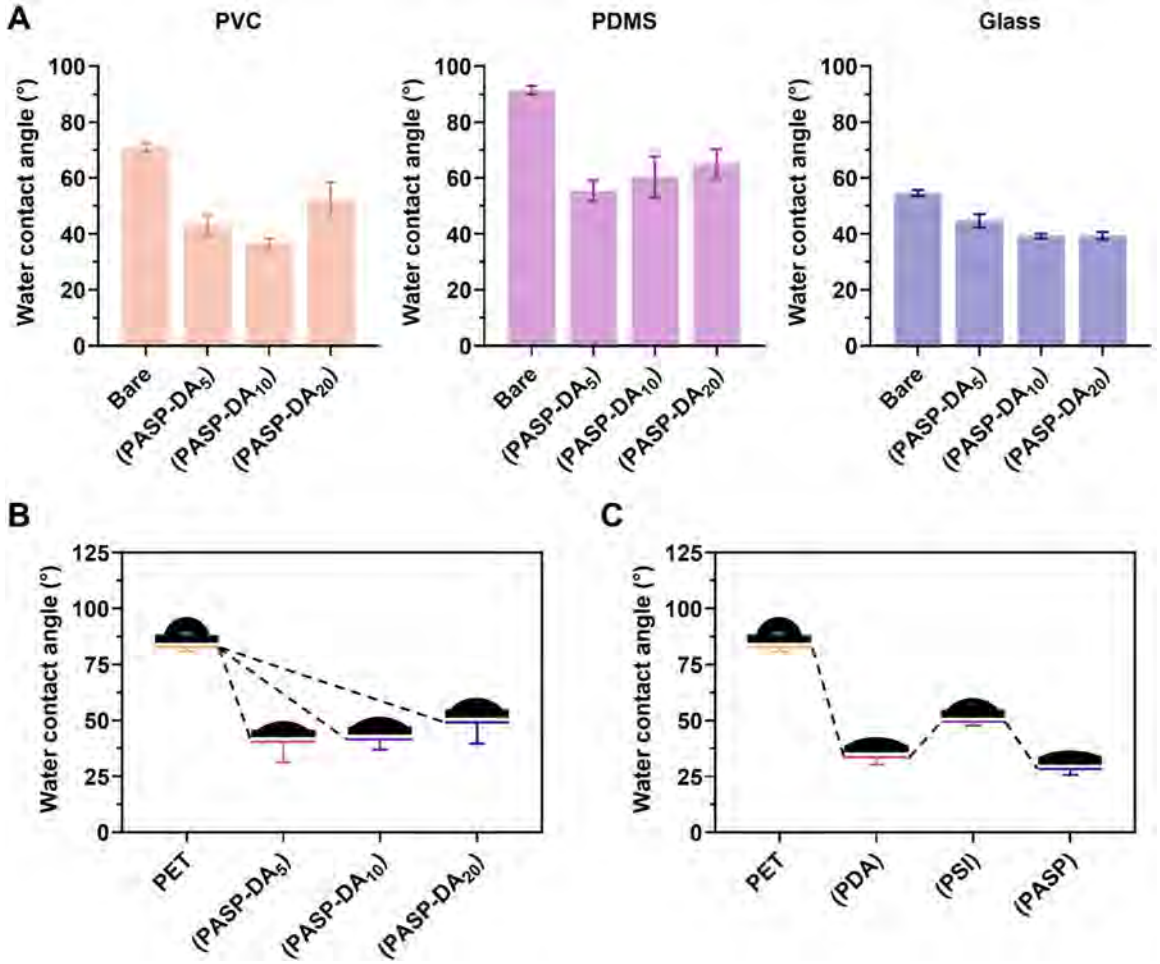

Fig. 3 Assessment of universal coating capabilities and refinement of coating techniques. (A) Water contact angle of surface coatings applied using the direct method on PVC, PDMS, and glass; comparison of water contact angles for surface coatings applied with the (B) direct method and (C) indirect method on PET substrates.

tension, exhibited a significant decrease following the direct coating process on PVC, PDMS, and glass. Similarly, Fig. 3B highlights the reduction in surface tension on PET, confirming the successful deposition of the coating on various substrates, irrespective of their inherent characteristics. However, no direct relationship was established between the DA content within the coating and the WCA, possibly due to the varied performance of the DA reaction on each material type. Nonetheless, these findings demonstrated the universal coating capabilities of DA, enhancing the surface coating process.

Regarding the "indirect method", PET was selected as the substrate to apply the coating and subsequently examine its properties, with the process outlined in Fig. S3. Here, the substrate was initially coated with a layer of polydopamine (PDA), leading to a notable reduction in surface tension, as evidenced by a decrease in WCA from 82.8 ± 0.6° to 33.7 ± 1.1°, as shown in Fig. 3C. Subsequently, PSI was applied through a ring-opening reaction of succinimide, resulting in a slight increase in WCA to 49.5 ± 0.6°. Given that PSI is not completely soluble in water and only dissolves in aprotic solvents, WCA slightly increases in this intermediate phase. The final stage involved the complete hydrolysis of the conjugated PSI in an alkaline medium, which reduced the WCA further to 28.4 ± 0.9°, marginally lower than that with PDA alone. This outcome demonstrates that the synergistic effect of PASP and PDA on the surface energy of the substrate is more pronounced than that observed with the direct method. Consequently, we have selected the indirect method as the preferable approach for conducting further in-depth studies.

3.4. Biocompatible characteristics of PASP surface coating

Coating confirmation. Following the preliminary validation of surface coatings through WCA measurements, we conducted further investigation to analyse their chemical bonding and to assess parameters indicative of surface anticoagulation ability and biocompatibility. The chemical structure of the material coated onto a PET sheet was first examined using FTIR, as depicted in Fig. 4A. The FTIR spectra, recorded after each coating step using the indirect method, are presented sequentially from top to bottom: PDA-, PSI- and PASP-coated

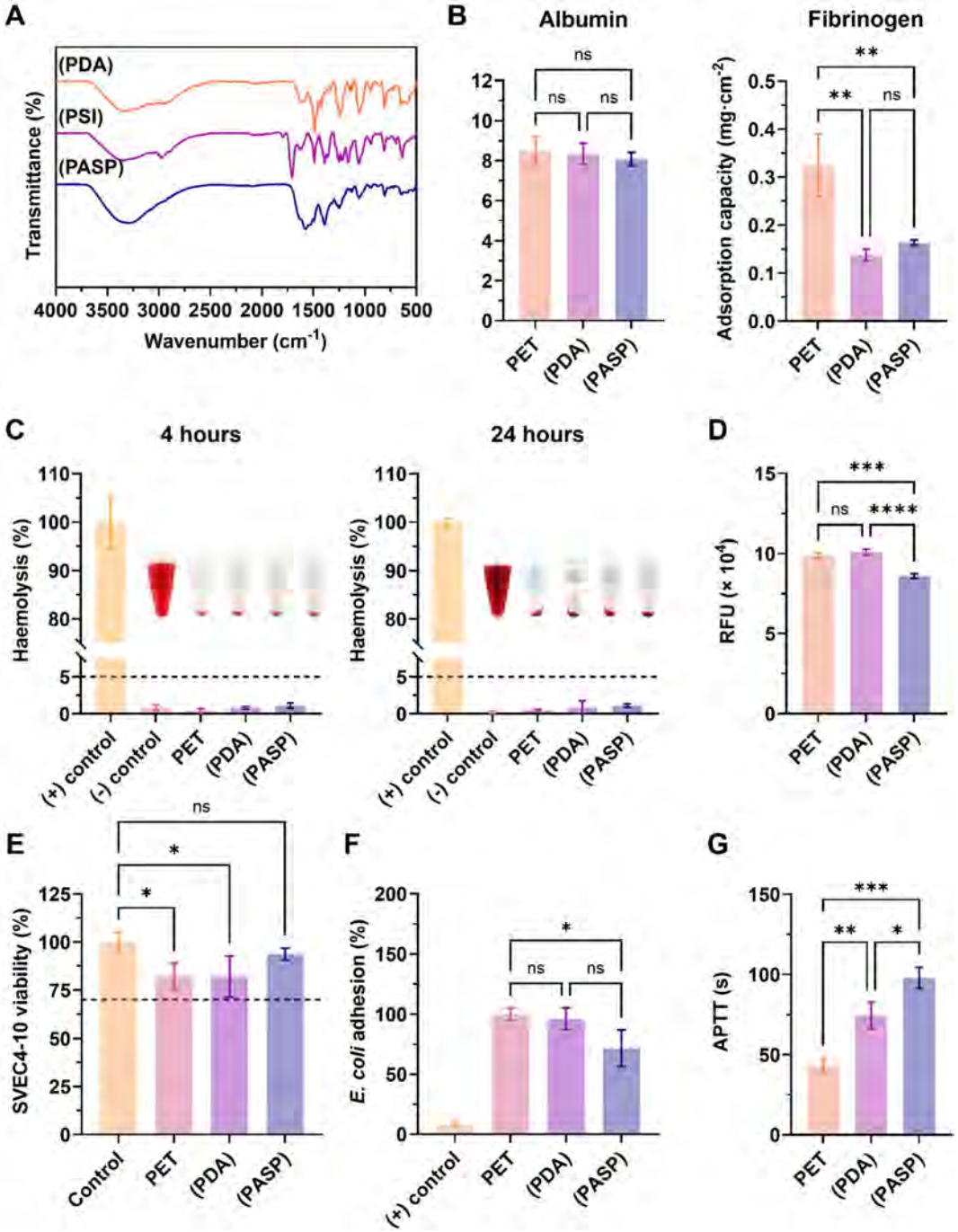

Fig. 4 Characteristics of PASP surface coating: (A) FTIR spectra of PDA-coated PET—namely (PDA), PSI-coated PET—namely (PSI), and PASP-coated PET—namely (PASP); (B) albumin and fibrinogen adsorption; (C) haemolytic activity; (D) platelet adhesion; (E) SVEC4-10 viability; (F) antibacterial efficacy; (G) APTT investigated in plain and coated surfaces.

sufarces are denoted as (PDA), (PSI), and (PASP), respectively. The FTIR spectrum of (PDA) displays absorption signals corresponding to N–H, O–H, and C–H stretching vibrations from catechol, methyl, and methine groups, observed from approximately 2800 cm^{-1} and higher. Additionally, the characteristic pattern of polydopamine below 1500 cm^{-1} is attributed to the stretching and bending vibrations of C═O and C–H. This pattern is similarly observed in the (PSI) spectrum following the deposition of the PSI layer onto the preceding PDA layer, alongside the appearance of the imide trough characteristic of the succinimide groups in PSI. Upon hydrolysis of the PSI layer, a marked increase in the O–H absorption trough indicates the formation of PASP. Similar patterns observed in the PASP and PDA spectra below 1500 cm^{-1} confirm the successful execution of the coating process, consistent with the previous WCA results.

Furthermore, the SEM images of the coated surfaces provided valuable insights. As shown in Fig. S5, the pristine PET surface, prior to coating, appeared relatively smooth. However, after deposition with PDA, the surface exhibited increased roughness, with PDA accumulating unevenly. This irregular distribution can be attributed to the formation of PDA nanoparticles both in the coating solution and on the coated surface.[46] Subsequently, after the PASP coating was applied, the polymeric layer evened out the surface, minimising the presence of particulate structures.

Protein adsorption. Testing protein adsorption with albumin and fibrinogen is essential for evaluating the surface blood clotting ability, as these proteins play critical roles in blood–material interactions. Albumin primarily inhibits non-specific protein adhesion and clot formation, whereas fibrinogen promotes clotting by facilitating platelet adhesion and aggregation, directly influencing surface thrombogenicity. As illustrated in Fig. 4B, the quantity of albumin adsorbed on the surface was relatively consistent across the three PET samples, (PDA), and (PASP), with values of 8.49 ± 0.57, 8.34 ± 0.45, and 8.09 ± 0.28 mg cm^{-2}, respectively. However, the amount of fibrinogen adhered to the surface varied significantly, with (PDA) and (PASP) adsorbing considerably less fibrinogen—0.13 ± 0.01 mg cm^{-2} and 0.16 ± 0.00 mg cm^{-2}, respectively—compared to PET, which adsorbed 0.32 ± 0.05 mg cm^{-2}. As noted earlier, while similar albumin adsorption levels may reduce the initiation of the coagulation cascade, fibrinogen has the opposite effect, triggering pathways that lead to blood clot formation. The ability of surface coatings to reduce fibrinogen adsorption may be attributed to increased surface energy, which facilitates the formation of a hydration layer that hinders the adsorption of hydrophobic segments on fibrinogen.

Platelet adhesion and coagulation. Platelets, being key agents in blood clotting, were also examined for their adhesion, as shown in Fig. 4D, providing further insights into the anticoagulant properties of the surface coatings. The results indicate a slight increase in platelet adhesion from 98 743.7 ± 1290.8 relative fluorescence unit (RFU) on bare PET to 101 081.3 ± 1428.0 RFU on PDA-coated PET. Conversely, the PASP-coated surface exhibited significantly lower platelet adhesion, at only 86 056.0 ± 1119.0 RFU.

Subsequently, activated partial thromboplastin time (APTT) was conducted to gain insight into the intrinsic coagulation pathway by measuring the time required for blood plasma to clot in response to specific activators (Fig. 4G). This assay aids in assessing the anticoagulant properties of a surface, determining whether it can prolong the clotting time and potentially reduce thrombus formation. The APTT results demonstrated that the (PDA) coating increased the clotting time to 74.3 ± 6.6 seconds, a finding consistent with previous studies, as PDA is known for its high biocompatibility. Moreover, the (PASP) coating extended the clotting time further to 97.7 ± 5.4 seconds, indicating PASP's effective regulation of the coagulation process and its potential to significantly reduce the risk of thrombus formation on coated surfaces. The surface anticoagulant mechanism of PASP was postulated to involve both the intrinsic and common coagulation pathways, as the results presented above demonstrated the coating's ability to attenuate surface contact activation and significantly prolong APTT.

Biocompatibility of PASP surface coating. Biocompatibility assessment is essential in surface coating research to ensure that materials do not elicit adverse biological reactions upon contact with tissues or blood. Haemolysis and cell viability assays are critical components of this evaluation, offering key insights into the potential for red blood cell damage and cytotoxicity. These tests confirm that the coating material is suitable for medical applications and does not compromise patient health. In this study, we conducted biocompatibility assessments using red blood cells and SVEC4-10, a representative endothelial cell line sensitive to blood-contacting devices. For the haemolysis assessment, Triton X-100 served as a positive control, while PBS was used as a negative control. The test samples, PET, (PDA), and (PASP), each with a diameter of 0.6 mm, were directly applied to the erythrocyte suspension, as shown in Fig. 4C. The results for 4 and 24 hours of incubation with red blood cells are relatively similar. Both coated and uncoated samples exhibited high haemocompatibility, with haemolysis rates below 2%, significantly lower than the ISO 10993-4:2017 standard threshold of 5%.[10]

Subsequently, cell compatibility was assessed by evaluating the viability of SVEC4-10 cells, which form the endothelial layer of blood vessels, thereby closely simulating the exposure of blood-contacting devices within the body. As shown in Fig. 4E, the coated samples displayed a significant reduction in viable cells compared to the untreated control. Cell viability for PET and (PDA) samples decreased to 82.3 ± 5.5% and 82.0 ± 8.7%, respectively. Conversely, PASP demonstrated relatively high cell viability with no significance compared to the control, at 93.7 ± 2.5%. Notably, all results were above 80%, which, according to ISO 10993-5:2009, indicates non-cytotoxicity, as cell viability above 70% is considered safe.[10] Consequently, PASP can be recognised as a safe material that does not induce cell death. The high compatibility of PASP with SVEC4-10 is particularly promising, as re-endothelialisation is a crucial factor for the long-term success of blood-contacting devices in clinical settings. Furthermore, while the non-coated PET surface induced a significant production of reactive oxygen species (ROS) by RAW 264.7 macrophages, both (PDA) and (PASP) coated ones did not, as presented in Fig. S9, demonstrating the biocompatibility of both (PDA) and (PASP) coatings. The low ROS production suggests a reduced inflammatory response in macrophages, minimising the risk of adverse effects when introduced into the body. Based on these evaluations, it is evident that PASP, when used as a surface coating, provides the proposed level of biosafety, highlighting its potential for application in blood-contacting devices.

Antibacterial efficacy of PASP surface coating. Infection is a common risk associated with blood-interacting devices in medical applications. Given the limited research on the antibacterial properties of PASP, we conducted a straightforward

test to evaluate the adhesion of *E. coli* on coated surfaces, comparing the results with uncoated PET, as illustrated in Fig. 4F. A positive control containing antibiotics was also included for reference. The results indicated a slight, though not significant, reduction in viable *E. coli* on PDA-coated surfaces, with a decrease to 96.2 ± 7.4% compared to the PET sample. However, the PASP-coated surface exhibited a more pronounced reduction, with bacterial adhesion dropping to 71.5 ± 12.6%. This reduction can be attributed to the increased surface energy and the negative charge of the PASP surface, which likely repels the negatively charged phospholipid membranes of bacteria. On the other hand, the results obtained

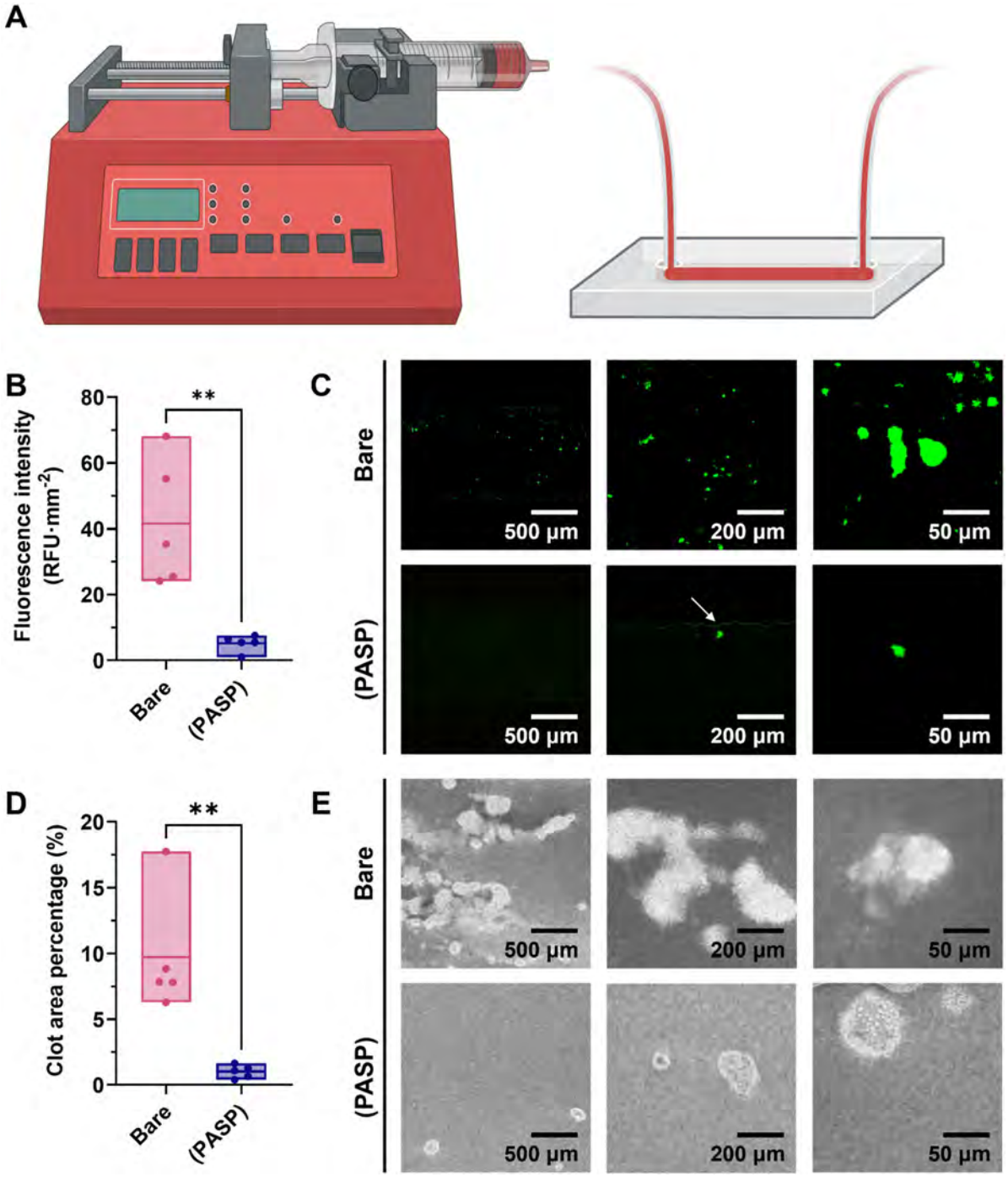

Fig. 5 *In vitro* antithrombotic studies. (A) Representation of antithrombotic assays on a microfluidic device model; (B) quantification of platelet adhesion on microfluidics from 5 fluorescence images; (C) fluorescence images at varying scale bars (platelets were labelled with DiOC6—green fluorescence), the white arrow points at the channel edge; (D) measurement of the thrombus area percentage from 5 distinct microscopic images; (E) microscopic images depicting thrombus formation on microfluidics.

against the Gram-positive bacterium *S. aureus* did not demonstrate a notably effective antibacterial response (Fig. S8), indicating that the antimicrobial capacity of PASP coatings remains limited in this context and warrants further investigation. However, it is crucial to note that this experiment serves as a proof-of-concept, where the material surface was exposed to a high concentration of bacteria over an extended period in conditions favourable for bacterial growth, making it challenging to compare directly with the antibiotic-positive control. Nonetheless, the observed inhibition of bacterial adhesion underscores the potential of PASP for antibacterial applications.

3.5. Platelet adhesion and thrombus formation under flow conditions

Several *in vitro* antithrombotic studies have been conducted on PASP-coated surfaces, comparing them with PDA intermediate coatings, and uncoated PET. However, it is important to note that blood-contacting devices are also influenced by the dynamic flow of blood, characterised by the shear rate. Numerous studies have indicated that the shear rate significantly impacts platelet stability, making platelets more sensitive and easily activated under its influence. Therefore, a microfluidic device model was employed to simulate the dynamics of blood flow, providing a more realistic assessment (Fig. 5A). Blood flow was calculated based on the theoretical viscosity of blood and the dimensions of the microfluidic device to replicate a physiological shear rate of approximately 1000 s^{-1} (refer to the SI).

The coating process was preliminarily evaluated by measuring the WCA on glass. As shown in Fig. S4, the WCA results on the glass substrate coated *via* the indirect method followed a similar trend to that observed on PET surfaces. After coating with PDA, the WCA decreased to 31.7 ± 1.2°, increased again to 42.7 ± 2.1° following the deposition of PSI, and finally decreased to 17.0 ± 0.8° after the hydrolysis of PSI to obtain (PASP). These results confirm the successful execution of the surface coating process, enabling further experimentation under dynamic flow conditions.

Once the coating was successfully applied, microfluidic devices with and without the coating were compared. The first experiment focused on platelet adhesion. Fluorescence microscopy images (Fig. 5C) revealed significant platelet attachment in the uncoated microfluidic device, with an uneven distribution likely due to platelet aggregation. High-magnification images clearly showed large clusters of aggregated platelets. In contrast, the PASP-coated channel surface exhibited minimal platelet adhesion, with visible platelets mostly confined to the channel edges, where rough and discontinuous areas resulted from plasma adhesion between the PDMS and glass substrate. Indeed, surface characteristics significantly influence platelet activation, as evidenced by these observations. Platelet adhesion evaluation was obtained by measuring the fluorescence intensity per area in five random images on three different channels at the highest magnification, with the results plotted in Fig. 5B. The uncoated surface had approximately 41.7 ± 19.3 RFU mm^{-2}, while the PASP-coated surface had only about 5.2 ± 2.5 RFU mm^{-2}, indicating that PASP substantially reduces platelet adhesion even under flow conditions.

In the thrombus formation experiment, thrombi were allowed to form on both coated and uncoated microfluidic devices. As shown in Fig. 5E, the uncoated microfluidic device displayed numerous clot formations, which tended to aggregate and form larger clots, clearly influenced by platelet aggregation activity. In contrast, the PASP-coated sample exhibited minimal thrombus formation, with clots that were generally small and discrete. Fig. 5D presents the quantitative results of thrombus formation by measuring the clot area using ImageJ software. The results, based on five images from three different channels, showed that the clot area percentage on the uncoated microfluidic device reached 9.7 ± 4.6%, significantly larger than the 1.0 ± 0.5% observed on the PASP-coated channel. These findings initially demonstrate that PASP holds great potential in preventing clot formation on surfaces, particularly in blood-interacting medical devices. Additionally, we successfully introduced a relatively effective and accessible *in vitro* evaluation method that offers a higher physiological correlation compared to conventional *in vitro* methods. While there are minor limitations that prevent direct comparison with *in vivo* conditions, this approach remains a valuable method for assessing antithrombotic surface coatings.

4. Conclusion

The present study demonstrated the optimisation of mussel-inspired methods with direct and indirect pathways for PASP coatings, with the indirect method proving superior due to its enhanced effects on surface energy and adhesion properties. PASP has shown significant potential in preventing blood clot formation on surfaces, as evidenced by *in vitro* experiments conducted under both static and dynamic flow conditions using a microfluidic device model. This innovative evaluation method not only simulated physiological conditions more accurately but also provided a reliable and accessible approach for assessing antithrombotic surface coatings. Moreover, preliminary tests indicated that PASP-coated surfaces exhibit antibacterial properties towards *E. coli*, further enhancing their potential application in medical devices where both blood compatibility and infection resistance are critical. Future research should focus on *in vivo* studies to validate these findings and explore the long-term stability and effectiveness of PASP coatings in clinical settings. Additionally, further exploration of PASP's antibacterial mechanisms could lead to the development of multifunctional coatings that provide comprehensive protection against thrombosis and infection in blood-contacting devices. Although PASP still has certain limitations and does not demonstrate groundbreaking antibacterial or anticoagulant properties, it remains a significant foundational material with the potential for further development and enhanced applications. Realising this potential will require more in-depth research in the future.

Author contributions

Cuong Hung Luu: writing – original draft, writing – review & editing, methodology, investigation, formal analysis, data curation, conceptualization, validation, and visualization. Dimple Sajin: methodology and investigation. Hoang Huy Vu: methodology and investigation. Nhat-Khuong Nguyen: methodology. Nam-Trung Nguyen: supervision and writing – review & editing. Hang Thu Ta: conceptualization, project administration, funding acquisition, methodology, supervision, and writing – review & editing.

Conflicts of interest

The authors declare that they have no conflict of interest.

Data availability

All data supporting the findings have been included in the articles. All raw data are included as part of the SI. See DOI: https://doi.org/10.1039/d4bm01714e.

Acknowledgements

This work is funded by Griffith University and the National Health and Medical Research Council (Hang Thu Ta: APP1182347, APP2002827). Hang Thu Ta is supported by the Heart Foundation Future Leader Fellowship (102761). Cuong Hung Luu's PhD scholarship is provided by Hang Thu Ta funding (102761) and Griffith University. We would like to acknolwedge Queensland Australian National Fabrication Facilities (ANFF) for access to some key instruments.

References

1 C. H. Luu, N.-T. Nguyen and H. T. Ta, *Adv. Healthcare Mater.*, 2024, **13**, 2301039.
2 D. C. Leslie, A. Waterhouse, J. B. Berthet, T. M. Valentin, A. L. Watters, A. Jain, P. Kim, B. D. Hatton, A. Nedder, K. Donovan, E. H. Super, C. Howell, C. P. Johnson, T. L. Vu, D. E. Bolgen, S. Rifai, A. R. Hansen, M. Aizenberg, M. Super, J. Aizenberg and D. E. Ingber, *Nat. Biotechnol.*, 2014, **32**, 1134–1140.
3 M. Ashcraft, M. Garren, O. Lautner-Csorba, V. Pinon, Y. Wu, D. Crowley, J. Hill, Y. Morales, R. Bartlett, E. J. Brisbois and H. Handa, *Adv. Healthcare Mater.*, 2024, **13**, 2400492.
4 P. L. Thi, T. Y. N. Tran, H. C. Luu, D. L. Tran, T. T. H. Thi and D. H. Nguyen, *J. Bioact. Compat. Polym.*, 2022, **37**, 252–266.
5 C. H. Luu, D. T. D. Nguyen, C. Y. Chee, T. C. N. Thi, D. Y. P. Nguyen, D. H. Nguyen and C. K. Nguyen, *J. Appl. Polym. Sci.*, 2023, **140**, e54108.
6 B. Tillman and D. Gailani, *Semin. Thromb. Hemostasis*, 2018, **44**, 060–069.
7 N. H. T. Luu, H. Q. Ly, C. V. Nguyen, L. T. T. Dinh, T.-K. N. Nguyen, C. M. Phan, M. L. Nguyen, H. H. Vu, C. H. Luu and T. T. Hoang Thi, *J. Polym. Sci.*, 2024, **63**, 541–553.
8 L. Witzdam, B. Vosberg, K. Große-Berkenbusch, S. Stoppelkamp, H. P. Wendel and C. Rodriguez-Emmenegger, *Macromol. Biosci.*, 2024, **24**, 2300321.
9 G. Apte, J. Börke, H. Rothe, K. Liefeith and T.-H. Nguyen, *ACS Appl. Bio Mater.*, 2020, **3**, 5574–5589.
10 P.-K. T. Ngo, D. N. Nguyen, H.-P. Nguyen, T.-H. H. Tran, Q.-N. D. Nguyen, C. H. Luu, T.-H. Phan, P. K. Le, V. H. G. Phan, H. T. Ta and T. Thambi, *Int. J. Biol. Macromol.*, 2024, **279**, 135329.
11 V. H. G. Phan, M. Murugesan, P. Manivasagan, T. L. Nguyen, T.-H. Phan, C. H. Luu, D.-K. Ho, Y. Li, J. Kim, D. S. Lee and T. Thambi, *Pharmaceutics*, 2022, **14**, 709.
12 V. H. G. Phan, M. Murugesan, P. P. T. Nguyen, C. H. Luu, N.-H. H. Le, H. T. Nguyen, P. Manivasagan, E.-S. Jang, Y. Li and T. Thambi, *Colloids Surf., B*, 2022, **219**, 112859.
13 Y. Jiang, H. Wang, X. Wang and Q. Li, *Int. J. Biol. Macromol.*, 2022, **219**, 1146–1154.
14 K. X. Vazquez-Prada, S. S. Moonshi, Y. Wu, K. Peter, X. Wang, Z. P. Xu and H. T. Ta, *Biomater. Sci.*, 2025, **13**, 1683–1696.
15 H. H. Vu, N.-T. Nguyen, N.-K. Nguyen, C. H. Luu, S. Hettiarachchi and N. Kashaninejad, *Adv. Eng. Mater.*, 2023, **25**, 2300821.
16 K. Zhang, T. Liu, J.-A. Li, J.-Y. Chen, J. Wang and N. Huang, *J. Biomed. Mater. Res., Part A*, 2014, **102**, 588–609.
17 L. Li, L. Yang, Y. Liao, H. Yu, Z. Liang, B. Zhang, X. Lan, R. Luo and Y. Wang, *Chem. Eng. J.*, 2020, **402**, 126196.
18 P. Lancellotti, A. Aqil, L. Musumeci, N. Jacques, B. Ditkowski, M. Debuisson, M. Thiry, J. Dupont, A. Gougnard, C. Sandersen, J.-P. Cheramy-Bien, N. Sakalihasan, A. Nchimi, C. Detrembleur, C. Jérôme and C. Oury, *J. Thromb. Haemostasis*, 2023, **21**, 2485–2498.
19 V. M. Ragaseema, S. Unnikrishnan, V. Kalliyana Krishnan and L. K. Krishnan, *Biomaterials*, 2012, **33**, 3083–3092.
20 L. Wang, H. Li, S. Chen, C. Nie, C. Cheng and C. Zhao, *ACS Biomater. Sci. Eng.*, 2015, **1**, 1183–1193.
21 S. S. Moonshi, K. X. Vazquez-Prada, H. Adelnia, N. J. Westra van Holthe, Y. Wu, J. Tang, A. C. Bulmer and H. T. Ta, *Appl. Mater. Today*, 2024, **37**, 102150.
22 H. Adelnia, H. D. N. Tran, P. J. Little, I. Blakey and H. T. Ta, *ACS Biomater. Sci. Eng.*, 2021, **7**, 2083–2105.
23 S. M. Thombre and B. D. Sarwade, *J. Macromol. Sci., Part A: Pure Appl. Chem.*, 2005, **42**, 1299–1315.
24 J. Shen, Z. Zhou, D. Chen, Y. Wang, Y. He, D. Wang and J. Qin, *Colloids Surf., B*, 2021, **200**, 111568.
25 H. Adelnia, S. S. Moonshi, Y. Wu, A. C. Bulmer, R. Mckinnon, J. W. Fastier-Wooller, I. Blakey and H. T. Ta, *ACS Nano*, 2023, **17**, 18775–18791.
26 X. Chen, S. S. Moonshi, N.-T. Nguyen and H. T. Ta, *Nanotechnology*, 2023, **35**, 055101.

27 S. S. Moonshi, K. X. Vazquez-Prada, H. Adelnia, N. J. Westra van Holthe, Y. Wu, J. Tang, A. C. Bulmer and H. T. Ta, *Appl. Mater. Today*, 2024, **37**, 102150.
28 H. A. Lee, Y. Ma, F. Zhou, S. Hong and H. Lee, *Acc. Chem. Res.*, 2019, **52**, 704–713.
29 G. Weaving, G. F. Batstone and R. G. Jones, *Ann. Clin. Biochem.*, 2016, **53**, 106–111.
30 G. D. Lowe, A. Rumley and I. J. Mackie, *Ann. Clin. Biochem.*, 2004, **41**, 430–440.
31 D. L. Tran, P. Le Thi, S. M. Lee, T. T. Hoang Thi and K. D. Park, *J. Controlled Release*, 2021, **329**, 401–412.
32 Y. Matsuhashi, K. Sameshima, Y. Yamamoto, M. Umezu and K. Iwasaki, *PLoS One*, 2017, **12**, e0188729.
33 M. A. O'Leary and G. K. Isbister, *J. Pharmacol. Toxicol. Methods*, 2010, **61**, 27–31.
34 C. M. Phan, C. H. Luu, M. Murugesan, T.-N.-Q. Nguyen, N.-Y. N. Ha, H. L. Ngo, N.-D. H. Nguyen, Z. Pan, V. H. G. Phan, Y. Li and T. Thambi, *Int. J. Biol. Macromol.*, 2025, **284**, 137939.
35 T.-H. H. Tran, C. H. Luu, K.-T. T. Nguyen, M.-A. L. Hoang, Q.-K. Pham, C. M. Phan, N.-K.-L. Thai, H. T. Nguyen, T. Thambi and V. H. G. Phan, *Macromol. Biosci.*, 2024, 2400351.
36 V. H. G. Phan, B.-P. T. Nguyen, N. Y. Nguyen, C.-N. D. Tran, Q.-N. D. Nguyen, C. H. Luu, P. Manivasagan, E.-S. Jang, D. C. Yang, D. U. Yang, Y. Li, J. Conde and T. Thambi, *Int. J. Biol. Macromol.*, 2025, **308**, 142254.
37 J. L. Tang, S. S. Moonshi, Y. Wu, G. Cowin, K. X. Vazquez-Prada, H. D. Tran, A. C. Bulmer and H. T. Ta, *Mater. Today Bio*, 2025, **30**, 101377.
38 Y. Wu, G. Cowin, S. S. Moonshi, H. D. Tran, N. A. Fithri, A. K. Whittaker, R. Zhang and H. T. Ta, *Mater. Sci. Eng., C*, 2021, **131**, 112477.
39 K. X. Vazquez-Prada, S. S. Moonshi, Y. Wu, F. Akther, B. W. Tse, K. A. Sokolowski, K. Peter, X. Wang, G. Xu and H. T. Ta, *Small*, 2023, **19**, 2205744.
40 Kenry, K. P. Loh and C. T. Lim, *Small*, 2015, **11**, 5105–5117.
41 H. Adelnia, I. Blakey, P. J. Little and H. T. Ta, *J. Mater. Chem. B*, 2023, **11**, 2650–2662.
42 D. Zhu, J. Guo, P. Yang, L. Pan, X. Zhong and S. Chen, *J. Appl. Polym. Sci.*, 2014, **131**, DOI: 10.1002/app.40282.
43 H. Adelnia, F. Sirous, I. Blakey and H. T. Ta, *Int. J. Biol. Macromol.*, 2023, **229**, 974–993.
44 N. R. Barros, Y. Chen, V. Hosseini, W. Wang, R. Nasiri, M. Mahmoodi, E. P. Yalcintas, R. Haghniaz, M. M. Mecwan, S. Karamikamkar, W. Dai, S. A. Sarabi, N. Falcone, P. Young, Y. Zhu, W. Sun, S. Zhang, J. Lee, K. Lee, S. Ahadian, M. R. Dokmeci, A. Khademhosseini and H.-J. Kim, *Biomater. Sci.*, 2021, **9**, 6653–6672.
45 C. Zhang, B. Wu, Y. Zhou, F. Zhou, W. Liu and Z. Wang, *Chem. Soc. Rev.*, 2020, **49**, 3605–3637.
46 M. Wu, T. Wang, L. Müller and F. A. Müller, *Colloids Surf., A*, 2020, **603**, 125196.

SUPPLEMENTARY INFORMATION

Polyaspartic Acid Coatings for Blood-Contacting Surfaces: Promising Antithrombotic and Antibacterial Properties under Static and Dynamic Conditions

Cuong Hung Luu [a,b], Dimple Sajin [a,b], Hoang Huy Vu [b,c], Nhat-Khuong Nguyen [b], Nam-Trung Nguyen [b], Hang Thu Ta [a,b,*]

[a] School of Environment and Science, Griffith University, Nathan, QLD 4111, Australia
[b] Queensland Micro- and Nanotechnology Centre, Griffith University, Nathan, QLD 4111, Australia
[c] School of Engineering and Built Environment, Griffith University, Nathan, QLD 4111, Australia

Calculation of flow rate in a microfluidic device based on physiological shear rate

The flow rate employed in microfluidic device studies is determined based on laminar and Newtonian flow dynamics. The single-channel dimensions of the microfluidic device were designed with a width of 255 μm, a height of 110 μm, and a length of 20 mm. For simplicity, we utilised a shear rate calculation method derived from previous literature. [1,2] The primary objective is to achieve a shear rate of 1000 s^{-1}, which closely approximates the physiological shear rate observed in most blood vessels, thereby allowing us to simulate the effect of flow on the surface coating as it would occur within the vasculature. In the case of a rectangular channel, the relationship between shear rate (γ) and flow rate (Q) can be estimated using Equation S1, where γ represents the shear rate in s^{-1}, Q is the flow rate in $m^3 \cdot s^{-1}$, w denotes the channel width in metres, and h signifies the channel height in metres.

$$\gamma = \frac{6Q}{w \cdot h^2} \tag{S1}$$

Given the specified dimensions of the microfluidic device, these measurements are first converted into metres:

$$w = 255\ \mu m = 255 \times 10^{-6}\ m$$

$$h = 110\ \mu m = 110 \times 10^{-6}\ m$$

By substituting the corresponding dimensions and the target shear rate of 1000 s^{-1} into the modified version of Equation S1 (Equation S2), we arrive at a calculated flow rate:

$$Q = \frac{\gamma \cdot w \cdot h^2}{6} \tag{S2}$$

$$Q = \frac{1000 \times 255 \times 10^{-6} \times \left(110 \times 10^{-6}\right)^2}{6} = 5.1425 \times 10^{-10}\ m^3 \cdot s^{-1}$$

The flow rate is then further adjusted through unit conversions to match the settings of the syringe pump in $\mu L \cdot min^{-1}$.

$$Q = 5.1425 \times 10^{-10}\, m^3 \cdot s^{-1} = 30.855\, \mu L \cdot min^{-1}$$

Consequently, a flow rate of 31 μL·min^{-1} was set on the syringe pump to approximately simulate a shear rate of 1000 s^{-1} within the dynamic flow environment of blood vessels using the specific microfluidic device.

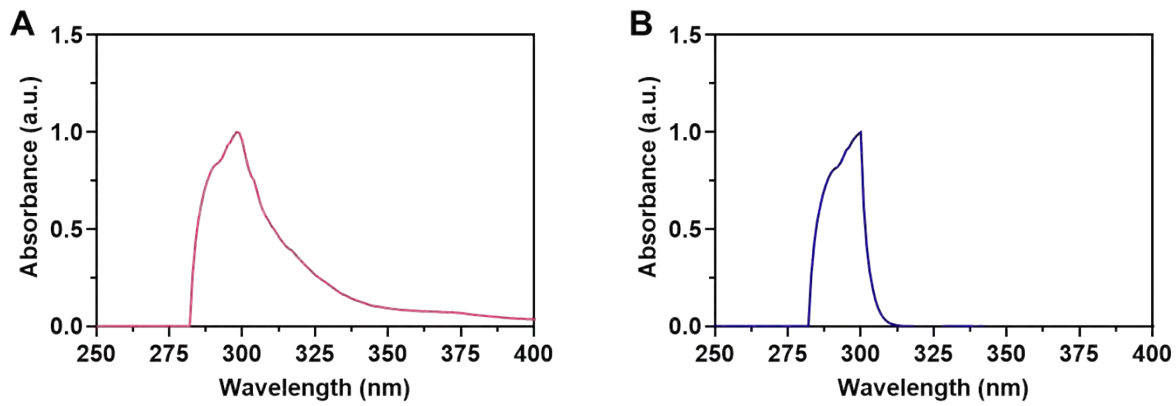

Figure S1. UV-Vis spectra of (A) PSI and (B) DA.

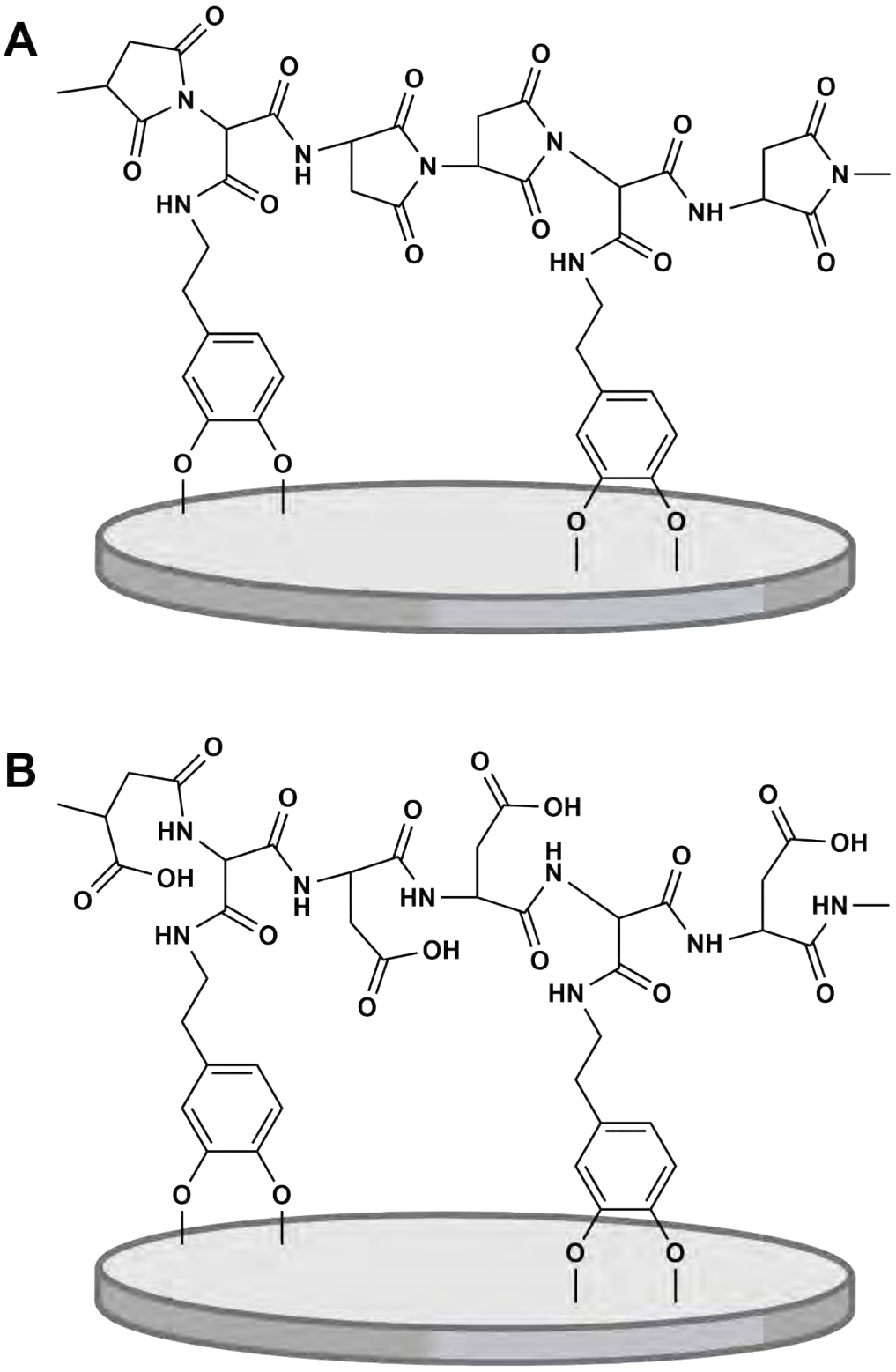

Figure S2. Schematic representation of surface coating preparation via direct method. (A) Substrate coated directly with PSI-DA in DMSO to form a (PSI) layer; (B) followed by hydrolysis in NaOH to produce a (PASP) coating.

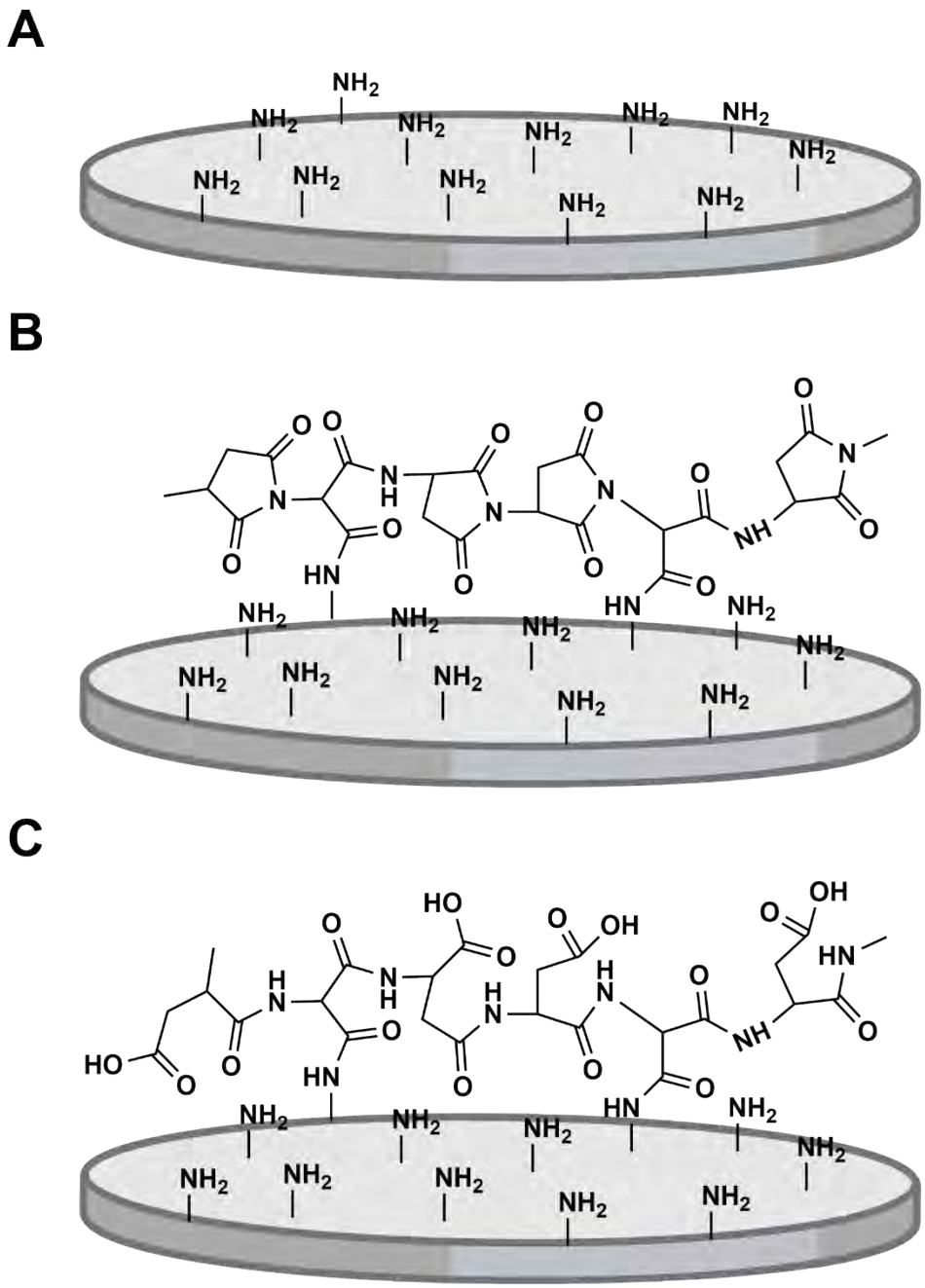

Figure S3. Schematic representation of surface coating preparation via indirect method. (A) The substrate is first coated with a layer of polydopamine (PDA), (B) followed by the deposition of the PSI polymer, which reacted with amine groups to form (PSI), (C) and subsequently hydrolysed to yield (PASP).

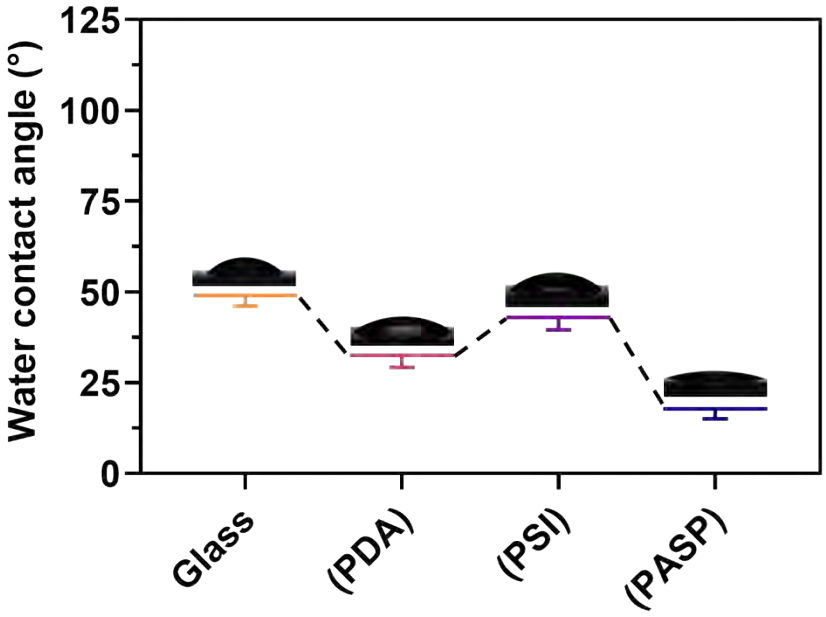

Figure S4. Water contact angle (WCA) of surface coatings on glass substrate via indirect method.

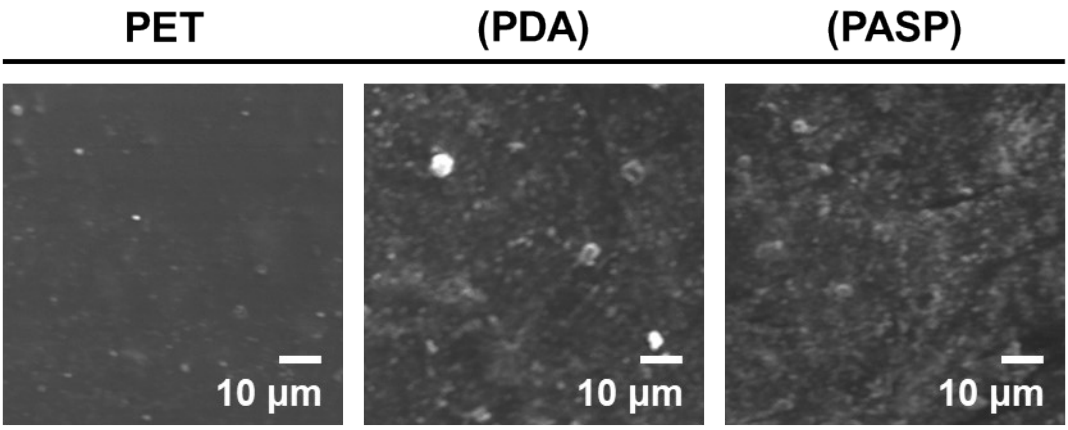

Figure S5. SEM images of PET, (PDA), and (PASP).

Hydrolysis of coated PSI

The hydrolytic stability of PSI was assessed by measuring its absorbance at 280 nm. A 96-well plate was used to coat PSI following the indirect method, in which polydopamine was first deposited onto the surface, followed by a layer of polysuccinimide. Sodium hydroxide was added to hydrolyse PSI layer into PASP. Polysuccinimide, which exhibits a characteristic absorbance peak at 280 nm due to the strong UV absorbance of the succinimide groups. Upon hydrolysis, these succinimide groups undergo ring-opening, converting into amide groups that do not exhibit significant absorption in the UV-Vis spectrum. Here, we measured the absorbance at the wavelength of 280 nm, the decrease in the intensity showed that there was hydrolysis process occurred. The results demonstrated a sharp decline in absorbance within the first 10 seconds, eventually decreasing to approximately zero, indicating that nearly all succinimide groups initially coated on the well plate surface had undergone complete hydrolysis.

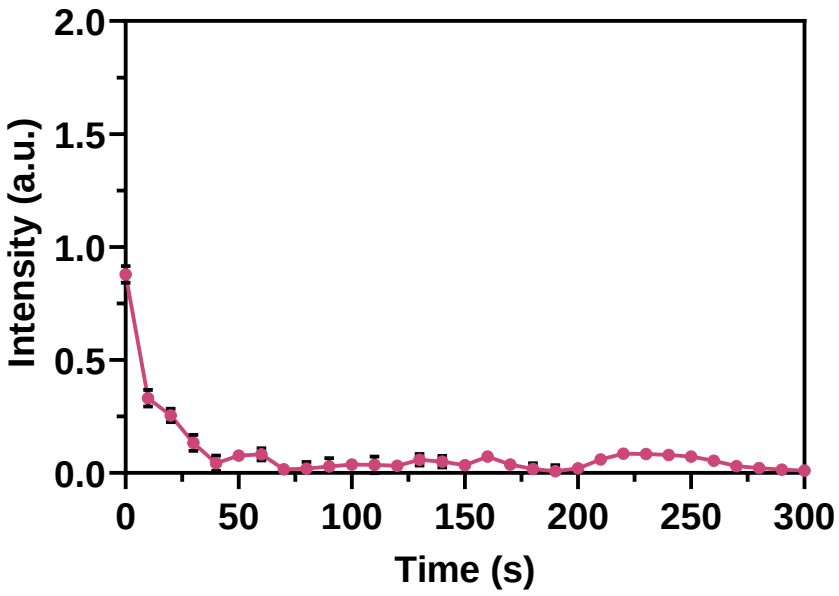

Figure S6. Hydrolysis of coated PSI recorded by the absorbance at 280 nm.

Coating stability

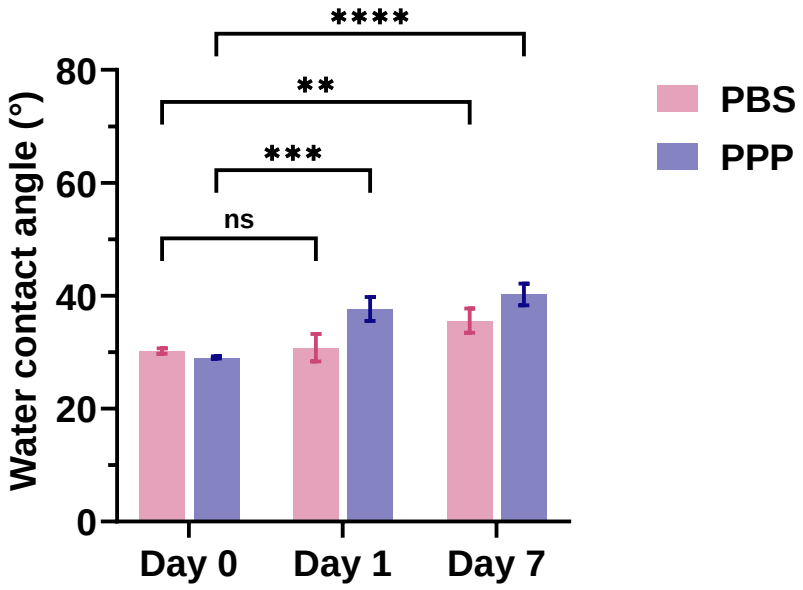

Figure S7. Coating stability of (PASP) under moderate shaking in PBS and PPP.

The stability of the coating was evaluated by immersing PASP-coated PET surfaces in either 1 mL of PBS buffer solution or platelet-poor plasma (PPP). These coated samples were then incubated in a shaking incubator at 37 °C and 500 rpm to simulate the dynamic forces that may act on the surface coating. After 1 and 7 days of incubation, WCA measurements were performed as an indicator of coating durability. The results demonstrated a gradual decrease in WCA over time, indicating a reduction in coating stability. Among the tested conditions, coatings immersed in PBS exhibited greater stability compared to those in PPP. This difference could be attributed to the presence of reactive components in PPP, such as degradative enzymes, which may accelerate PASP degradation on the surface. However, despite this decline, the surface remained highly hydrophilic, suggesting a relatively stable coating under the tested conditions.

Gram-positive bacteria anti-adhesion

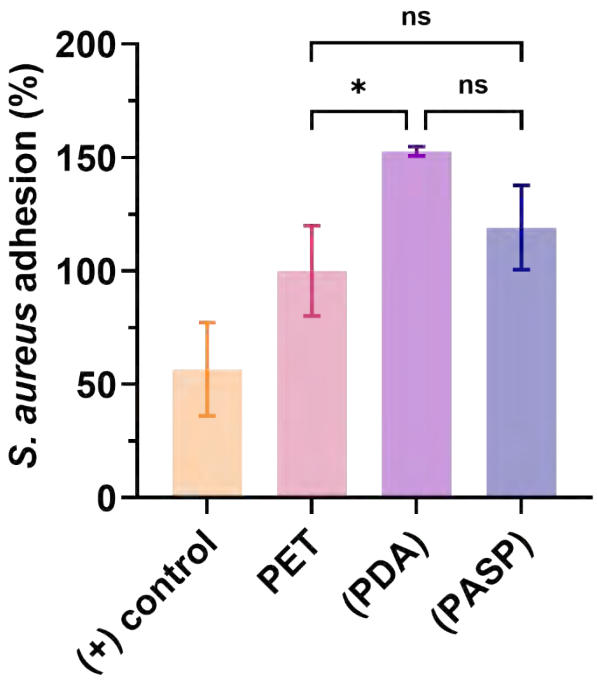

Figure S8. *S. aureus* anti-adhesion of (PASP) coating.

ROS induction level on RAW264.7

Macrophages (RAW 264.7, ATCC TIB-71) were used to evaluate the inflammatory response of the material, as they serve as the first line of defence in the immune system. In this experiment, coated materials were placed at the bottom of the wells in a 96-well plate, with empty wells serving as the control. 1×10^4 cells were then added into each well. After 24 hours, the reactive oxygen species (ROS) generated in the macrophages were assessed using the fluorescent dye 2',7'-dichlorodihydrofluorescein diacetate (DCFDA). Specifically, the cell culture medium was discarded, and wells were subsequently incubated with 100 µL of DCFDA solution at a concentration of 25 µM at 37 °C for 30 minutes. The fluorescence intensity measured by the spectrophotometer indicated the ROS production levels in RAW 264.7 cells.

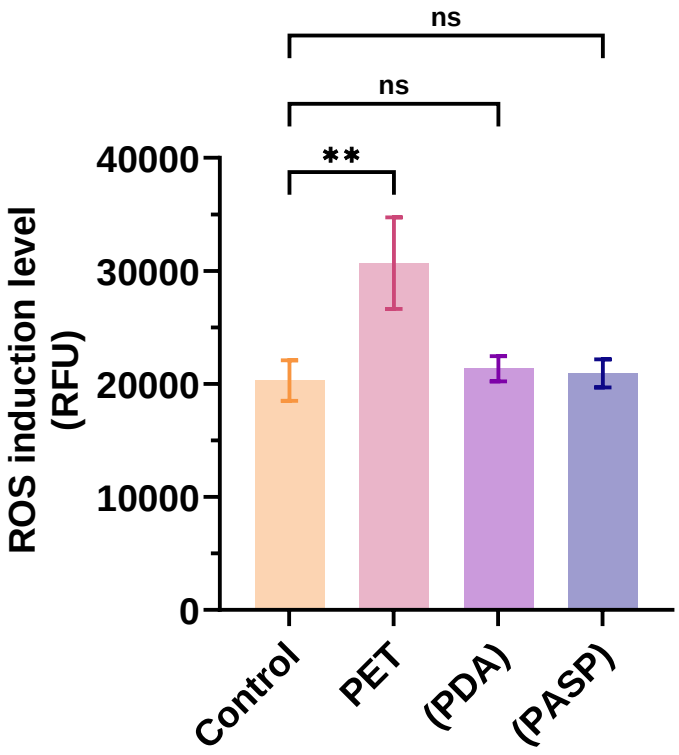

Figure S9. ROS induction level by RAW 264.7 macrophages when incubated with surface coatings.

References

1. F. Akther, J. Zhang, H. D. N. Tran, H. Fallahi, H. Adelnia, H.-P. Phan, N.-T. Nguyen and H. T. Ta, *Adv. Biol.*, 2022, **6**, 2101316.

2. Y. C. Zhao, P. Vatankhah, T. Goh, R. Michelis, K. Kyanian, Y. Zhang, Z. Li and L. A. Ju, *Sci. Rep.*, 2021, **11**, 6875.